

RESEARCH PAPER

The Effect of Terbium Dopant on Structural Characteristics of Zinc Tungstate

Gholamreza Gholami ¹, Morteza Raeisi ¹, Sanaz Alamdari ^{2*}, Nooshin Heydarian Dehkordi ²

¹Department of Physics, Faculty of Science, Shahrekord University, Shahrekord, Iran

²Department of Nanotechnology, Faculty of New Sciences and Technologies, Semnan University, Semnan, Iran

ARTICLE INFO

Article History:

Received 05 Aug 2023

Accepted 18 Sep 2023

Published 01 Jan 2024

Keywords:

ZnWO₄,

Terbium-doped ZWO,

Nanoparticles,

Crystal structure.

ABSTRACT

Zinc tungstate (ZnWO₄) possesses exceptional optical properties, making it a valuable material for scintillators and phosphors in radiation detection and imaging applications. Its high density and excellent light yield contribute to its effectiveness in capturing and converting ionizing radiation into detectable signals with precision. In this study, the pure (ZWO) and terbium-doped ZWO nanoparticles (ZWO: Tb) were synthesized using a simple co-precipitation method. X-ray diffraction (XRD), Fourier Transform Infrared (FTIR), and Field-Emission Scanning electron microscope (SEM) were used to characterize the crystal structure, binding vibrations, and morphology of the prepared nanopowders, respectively. The prepared nanoparticles were in a monoclinic wolframite phase with spherical, cubic, and planar (sheet-like) morphologies as well as the average particle size of 256.8 nm. Based on the FTIR results, the characteristic bands of Zn-O, Zn-O-W, and W-O bonds appeared at 428, 716, and 697 cm⁻¹, respectively. The prepared nanopowders can be advantageous for manufacturing flexible fluorescence materials, optoelectronic devices, and detectors.

How to cite this article

Gholami G., Raeisi M., Alamdari S., Heydarian Dehkordi N., *The Effect of Terbium Dopant on Structural Characteristics of Zinc Tungstate*. Nanochem. Res., 2024; 9(1): 35-41. DOI: 10.22036/NCR.2024.01.05

INTRODUCTION

Zinc tungstate is an inorganic material with a monoclinic wolframite phase structure of the P2/c space group [1]. The constitutive groups of the ZnWO₄ structure include distorted octahedra [ZnO₆] and [WO₆] that create structural defects in the network [2]. The schematic diagram of the wolframite-type monoclinic structure of the ZnWO₄ single crystal is shown in Fig. 1.

As presented in Fig.1, the WO₆ octahedron includes two O₂ and four O₁ atoms, whereas the ZnO₆ octahedron comprises four O₂ and two O₁. The bond lengths of W-O₁, W-O₂, Zn-O₁, and Zn-O₂ are equal to 2.136 Å, 1.579 Å, 1.77 Å, and 2.27 Å, respectively [4]. The bond lengths of W-O₁-Zn, W-O₂-Zn, O₁-W-O₁, and O₂-W-O₂ are equal to 128.136 Å, 129.76 Å, 164.268 Å, and 106.643 Å,

respectively [4]. ZWO is a self-activating phosphor with intrinsic bluish-green emission broadband under UV excitation [5], high light yield [6], high thermal and chemical stabilities, high average refractive index [7], and non-toxicity. The optical properties of tungstate compounds can be tuned by adjusting the temperature and rare earth (RE) dopant ions [5-7]. For example, doping with Tb³⁺ and Eu³⁺ can produce green and red-emitting phosphors based on only one host material, namely ZWO [5]. The concentration of rare earth ions affects various properties of the ZWO phosphor, including their average particle size, band gap, and photoluminescence spectra intensity [5-8]. Zinc tungstate and rare earth ions have the same energy levels. Therefore, energy can be effectively transferred from the excited tungstate group to the rare earth ions [9]. High quantum efficiency

* Corresponding Author Email: s.alamdari@semnan.ac.ir



This work is licensed under the Creative Commons Attribution 4.0 International License.

To view a copy of this license, visit <http://creativecommons.org/licenses/by/4.0/>.

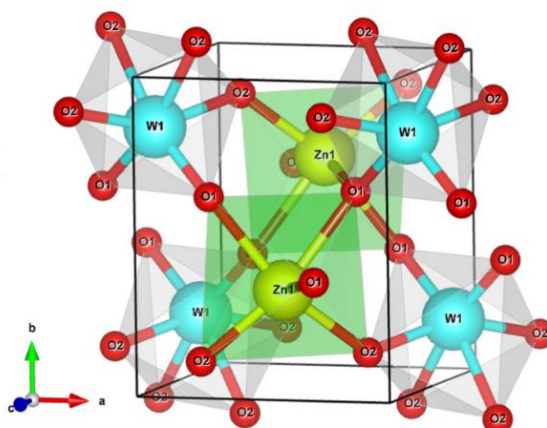


Fig. 1. Schematic diagram of wolframite type monoclinic structure of ZnWO_4 single crystal [3].

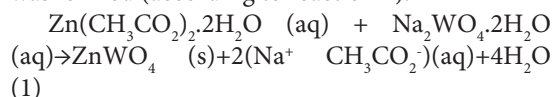
and high stability are characteristics of Tb^{3+} that produce green light, owing to the $^5\text{D}_4 \rightarrow ^7\text{F}_j$ ($J = 3, 4, 5, 6$) transitions [10]. The most common application of Tb^{3+} is in green phosphors and light-emitting diodes (LEDs) [9]. Until now, many studies have focused on the optical properties of rare earth metals such as Sm^{3+} [11] and Eu^{3+} [6], whereas there has been few research on the structure and characteristics of Tb^{3+} dopant. One method of preparing ZWO is crystal growth, but this method is costly, time-consuming, and requires advanced devices [12]. Nanocrystalline semiconductors have prominent luminescent properties owing to the quantum confinement effect [13]. ZWO nanoparticles can be quickly prepared using nanoscience and chemical synthesis methods such as sol-gel [14], co-precipitation [15], hydrothermal [6], solvothermal [16], and spray pyrolysis [17]. Linlin et al. synthesized two single-phase ZnWO_4 : RE^{3+} , Li^+ ($\text{RE} = \text{Sm}, \text{Eu}$) white phosphors by solid-state reaction [18]. Meiting et al. tailored the morphology of ZnWO_4 crystallites/Architectures and Photoluminescence of the doped RE^{3+} ions ($\text{RE} = \text{Sm}, \text{Eu}, \text{Tb}, \text{and Dy}$) synthesized by hydrothermal crystallization [19]. Azadmehr et al. reported the scintillation response of ZWO- graphene oxide (GO) nanocomposite synthesized by co-precipitation method [15]. Yequiu et al. reported the photocatalytic activities of ZnWO_4 and Bi@ZnWO_4 nanorods [20]. Madadi Mahani studied the photocatalytic activity of ZWO: Li by First-principles calculations according to density function theory (DFT) [21]. Brik et al. calculated the electronic and optical properties of CdWO_4 and ZnWO_4 using plane wave-based first-principles calculations [22]. Although many researchers have

investigated ZWO-doped with various rare earth elements [22-24], limited research has focused on the facile production of ZWO doped with Tb. In this study, ZWO, ZWO: 0.5at. % Tb and ZWO: 1at. % Tb nanocrystals were synthesized and their structural properties were characterized.

EXPERIMENTAL

Synthesis of Nanoparticles

ZWO, ZWO: 0.5 at. % Tb and ZWO: 1 at. % Tb nanocrystals were prepared by the co-precipitation method through the reaction of $\text{Zn}(\text{CH}_3\text{CO}_2)_2 \cdot 2\text{H}_2\text{O}$ (German Merck 99.99% purity), $\text{Na}_2\text{WO}_4 \cdot 2\text{H}_2\text{O}$, and $\text{Tb}(\text{NO}_3)_3 \cdot 6\text{H}_2\text{O}$ (Sigma Aldrich 99.99% purity) in deionized (DI) water. First, an equal number of moles of sodium tungstate dihydrate, zinc acetate dihydrate, and the corresponding amount of $\text{Tb}(\text{NO}_3)_3 \cdot 6\text{H}_2\text{O}$ were dissolved separately in DI water. After the complete dissolution of the above materials in DI water at ambient temperature, sodium tungstate solution was added dropwise to zinc acetate solution (the above operations were performed on a magnetic stirrer). After the above solutions were well mixed, a tungstate precipitate was formed (according to reaction 1).



The precipitation was washed 4 times with DI water and ethanol by centrifuge. The product was dried for 12 hours at 80°C and then calcined for 2 hours at 600°C . Finally, powders were prepared.

Characterization

X-ray diffraction (XRD) analyses (Bruker D8 diffractometer with $\text{Cu K}\alpha$ ($\lambda = 1.54 \text{ \AA}$)) were

applied to recognize the purity, phase, and crystal structure. Fourier Transform Infrared (FTIR) was carried out to characterize the bending and stretching vibrations of Zn-O, Zn-O-W, and W-O bonds. Field-Emission Scanning electron microscopy (FESEM- MIRA III TESCAN) exhibited the morphology and size of nanoparticles.

RESULTS AND DISCUSSION

Crystal Structure

Fig. 2 represents the XRD pattern of the as-synthesized ZnWO_4 and ZnWO_4 : (0.5 at. % & 1at. %) Tb^{3+} nanopowders in comparison to the standard card (JCPDS: 01-088-0251).

According to Fig. 2 (a), the diffraction peaks of samples are consistent with the reference code (JCPDS: 01-088-0251). Therefore, they have a monoclinic wolframite crystal structure with a space group of P2/c. The XRD pattern of ZWO and ZWO: 1 at.% Tb^{3+} nanopowders demonstrated excess peaks signed with circles corresponding to the low number of tungsten oxides [25]. According to Fig. 1 (b), the original diffraction peaks in the wolframite structure ((111) and (-111)) in the samples doped with Tb^{3+} shifted to higher angles. This shift can be attributed to the reduction in the distance between the crystal planes of ZWO (lattice contraction). The ionic radii of Tb^{3+} , Zn^{2+} , and W^{6+} for a coordination number of 6 are 0.092, 0.09, and 0.074 nm, respectively [26-28]. Thus, due to the similarity of their ionic radii, Tb^{3+} preferably replaces Zn^{2+} in the crystal lattice of ZWO. However, to balance the electric charge, 2/3 Tb^{3+} ion replaces one Zn^{2+} ion, thus causing contraction in the lattice and reducing the distance between

crystal planes. The intensity of the original peaks ((-111) and (111)) in doped samples decreases. Tb^{3+} affects the crystallinity and luminescent properties of ZWO [9]. The crystallite size and lattice strain were calculated using the Williamson-Hall method shown in Fig. 3.

According to Fig. 3, the crystallite size of ZWO: 1at. % Tb decreased, while the crystallite size of ZWO: 0.5at. % Tb sample increased. The lattice strain and distortion of the ZWO: 0.5at. % Tb was the highest value, while the ZWO: 1at. % Tb was the lowest. As soon as a small amount of Tb was added to the ZWO crystal structure, a large amount of distortion was created in the lattice, while the distortion decreased with the rise in the dopant percentage. The addition of the 0.5at.% Tb^{3+} to ZWO prepared the supersaturated solid solution and seeds of the secondary sediment phase. In addition, the host-sediment interface was incoherent with large incoherency. Therefore, the energy of the system and the strain increased (Fig. 3(b)). With the increase in the dopant percentage (the sample doped with 1 %at. Tb) and the enlargement of the sediment particles at the coherent interface created between the deposit and the host resulted in reducing both the energy of the system and the lattice strain, as depicted in Fig. 3(c).

FTIR spectroscopy

FTIR was applied to investigate the vibrational frequency of W-O, Zn-O, and Zn-O-W bonds. FTIR spectrum of ZWO, ZWO: 0.5 at. % Tb and ZWO: 1 at. % Tb powders are given in Fig. 4.

According to Fig. 4, eight vibration modes in the fingerprint region of the infrared spectra

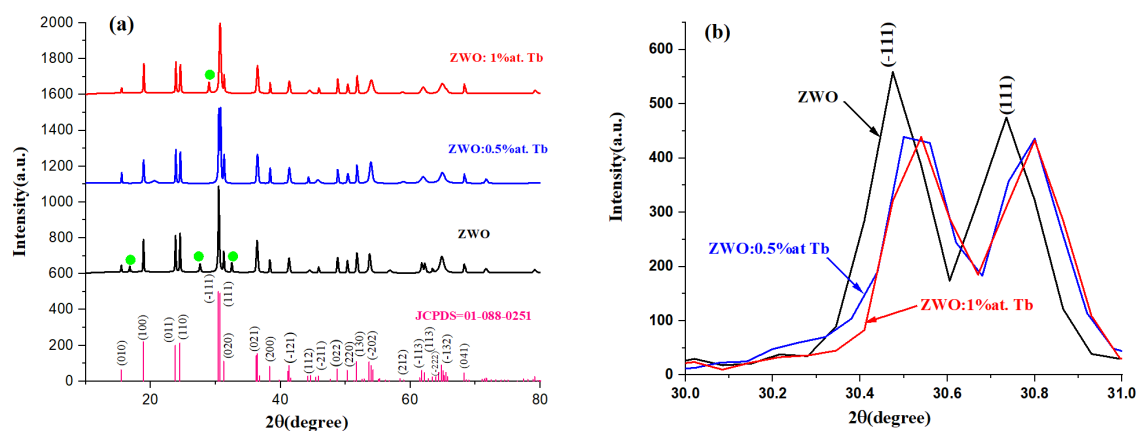


Fig. 2. (a) XRD pattern of ZWO, ZWO: 0.5 at. %, and ZWO: 1 at. % Tb nanopowder, and reference data of ZWO (JCPDS: 01-088-251). (b) A comparison between (-111) and (111) diffraction peaks.

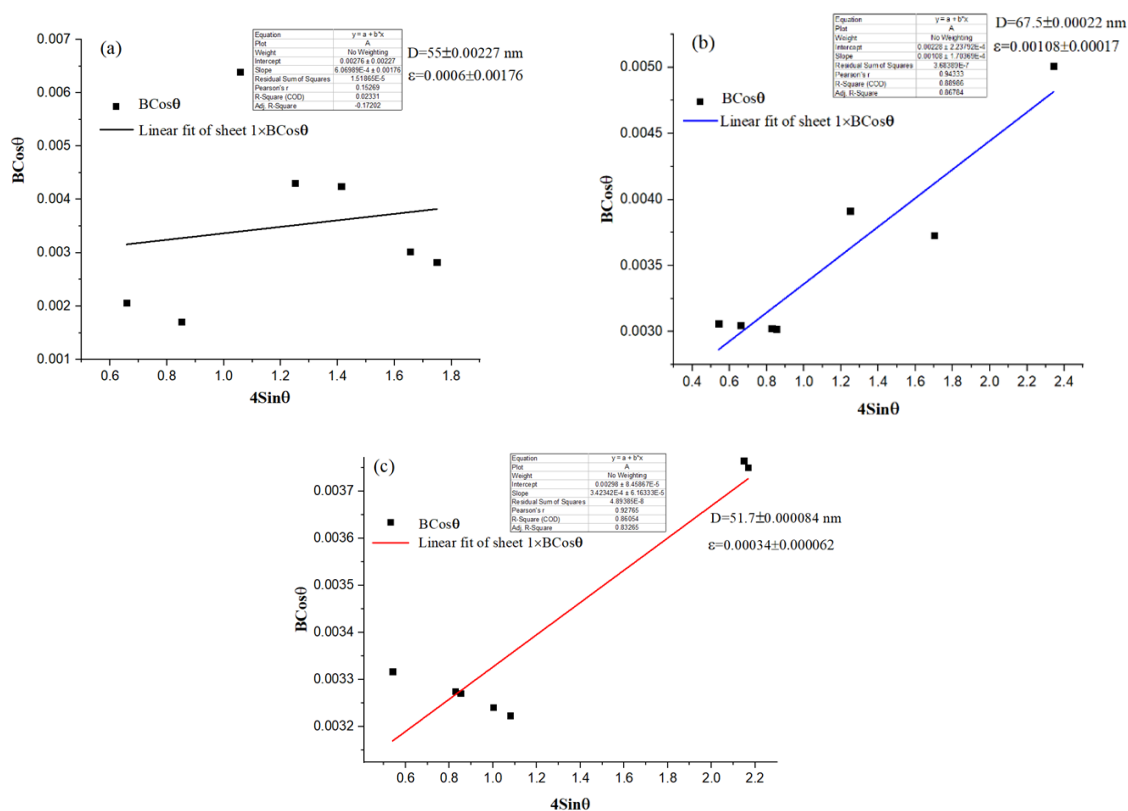


Fig. 3. Williamson-Hall plot ($Bcos\theta$ versus $4Sin\theta$) for (a) ZWO, (b) ZWO: 0.5 at. %Tb, and (c) ZWO: 1 at. % Tb nanopowders.

(1600-400 cm^{-1}) correspond to W-O and Zn-O vibrations. The bands at 428 cm^{-1} and 472 cm^{-1} are related to the banding and stretching vibrations of Zn-O, respectively, consistent with the results (432 and 473 cm^{-1}) presented in the articles [29] and [30]. Three bands at 532.32, 697, and 716 cm^{-1} are attributed to the symmetric and asymmetric stretching vibrations of bridging atoms in WO_2 groups of distorted octahedra (WO_6)⁶⁻, which are in agreement with the results (541, 685 and 716 cm^{-1}) reported in the articles [31] and [32]. 532.32 cm^{-1} and 716 cm^{-1} bands can be ascribed to the symmetric vibrations of the bridging oxygen atoms in the Zn-O-W group, in line with the results (710 and 540 cm^{-1}) mentioned in the articles [33]. Symmetric vibrations of bridging oxygen atoms of the Zn-O-W group caused broad absorption bands at 833.19 and 873 cm^{-1} [31]. Two vibrational modes at 1633.59 and 3460.06 cm^{-1} correspond to the bending and stretching vibrations of the OH group, respectively. It has been reported that the bending and stretching vibrations of the OH group are located at 1644 and 3448 cm^{-1} [9, 32]. The powders were hydroxylated. According to Fig. 4 (b), no significant displacement was observed in

the location of the transmittance bands of all three samples. The transmittance of doped samples, especially ZWO: 1at. % Tb in the near-infrared region (4000-11094 cm^{-1}) enhanced. Transmission in the pure sample was lower due to having more bonds in this frequency region. It seems ZWO has better luminescence and scintillation characteristics due to better crystallinity. The transmission value of doped samples, especially ZWO: 0.5at. % Tb in 428-873 cm^{-1} reduced. The number of Zn-O-W and W-O bonds was increased in doped samples. No significant displacement was observed in the location of the transmittance bands of all samples.

Morphology

In this part, using a Field-Emission Scanning Electron Microscope (FE-SEM), the shape, size, and size distribution of particles are examined. The results of FE-SEM and EDAX-map of ZWO: 1 at. % Tb nanoparticles are shown in Fig. 5.

According to the FE-SEM images, the morphology of ZWO: 1 at. % Tb nanoparticles were sheet-like, cubic, spherical, and rarely agglomerated in some parts with an average size of 256.8 nm. According to the EDS-map

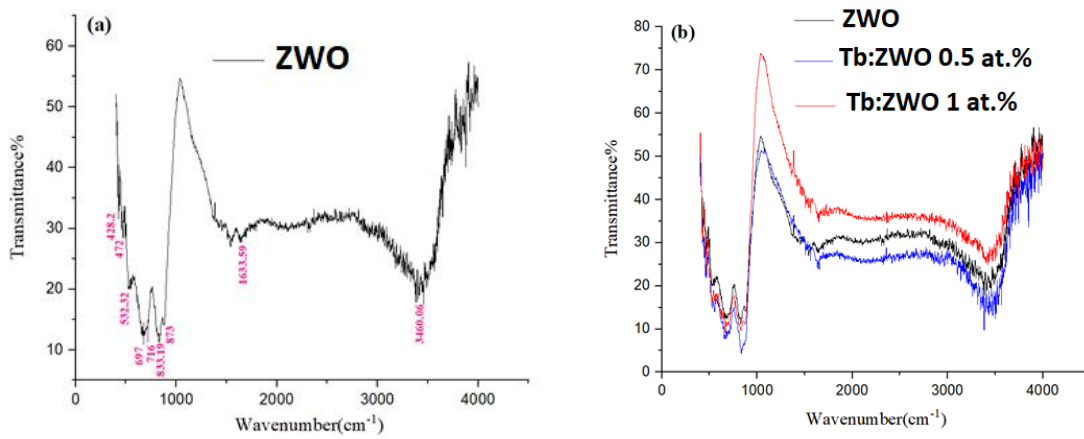


Fig. 4. FTIR spectra of (a) ZWO, (b) ZWO, ZWO: 0.5 at. % Tb, and ZWO: 1 at. % Tb nanopowders.

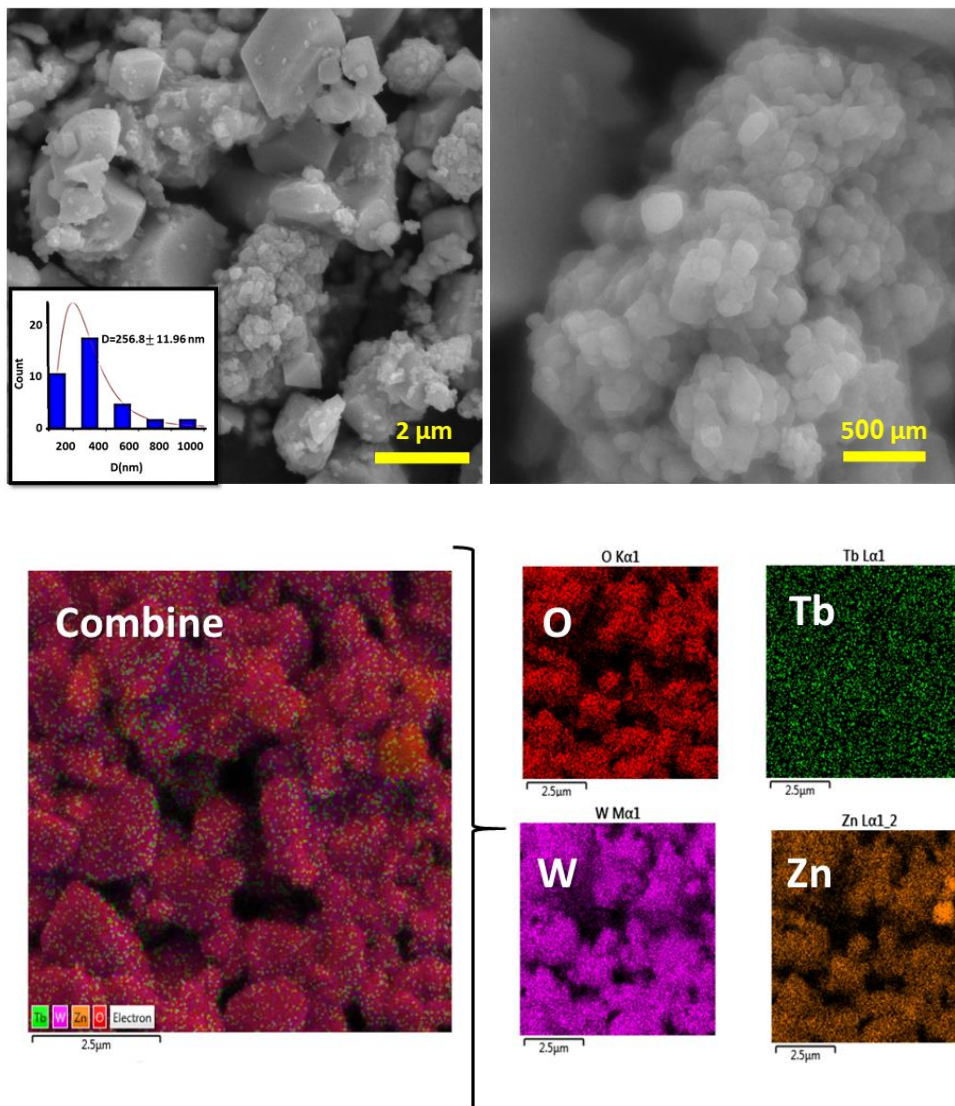


Fig. 5. FE-SEM and EDS-map images of ZWO: 1 at. % Tb nanoparticles with a histogram of particle size distribution.

images, the Tb distribution was uniform. The distribution of Zn, W, and O atoms is almost similar and non-uniform. In previous works, novel optical/structural properties were also observed in tungstate compound families [34-37]; therefore, facile prepared ZWO: Tb nanopowders can be advantageous for manufacturing flexible fluorescence materials, optoelectronic devices, and detectors in future.

CONCLUSION

In this work, the pure and Tb-doped zinc tungstate nanoparticles with different percentages of Tb³⁺ ions were prepared by a rapid and cost-effective co-precipitation method. The results of XRD demonstrated that the products have wolframite structure. The size of the crystallite size in the ZWO:0.5 at. % Tb was 67.5 nm, which was larger than that of other two samples. The results showed that the ZWO:1at. % Tb nanoparticles were flat and cubic with dimensions of 256.8 nm. The FTIR results indicated no significant change in terms of bond strength. However, the number of bonds (in the near-infrared region) decreased in ZWO:1at. % Tb sample, while it increased in ZWO:0.5 at. % Tb sample. The prepared powders can be advantageous for manufacturing flexible fluorescence materials, optoelectronic devices, and detectors.

CONFLICT OF INTEREST

The authors declare no conflicts of interest.

REFERENCES

- Madani M, Mansourian M, Alamdari S, Mirzaee O, Jafar Tafreshi M. Facile Synthesis and Characterization of Highly Luminescent Bi₂WO₆ Nanoparticles for Photonic Application. *Nanochemistry Research*. 2022;7(1):15-21.
- Gouveia AF, Assis M, Cavalcante LS, Gracia L, Longo E, Juan A. Reading at exposed surfaces: theoretical insights into photocatalytic activity of ZnWO₄. *Frontier Research Today*. 2018;1:1005. <https://doi.org/10.31716/frt.201801005>
- de Araújo LNM, Sousa BS, de Araújo AGE, Monção RM, Feitor MC, Sczancoski JC, et al. ZnWO₄ nanocrystals prepared by thermal plasma processing. *Journal of Materials Science*. 2023;58(16):6944-71. <https://doi.org/10.1007/s10853-023-08444-0>
- Heydarian Dehkordi N, Raeisi M, Alamdari S. The structural and optical behavior of Ag⁺ and Gd³⁺ ions in CdWO₄. *Nanochemistry Research*. 2022;7(1):53-61.
- Hosseinpour M, Mirzaee O, Alamdari S, Menéndez JL, Abdoos H. Development of a novel flexible thin PWO(Er)/ZnO(Ag) nanocomposite for ionizing radiation sensing. *Journal of Alloys and Compounds*. 2023;967:171678. <https://doi.org/10.1016/j.jallcom.2023.171678>
- Mansourian M, Alamdari S. Fabrication and Investigation on Luminescence Properties of Bi₂WO₆ Microfibers via Stretching Process. *Progress in Physics of Applied Materials*. 2023;3(Special Issue in Honor of Professor Perumalsamy Ramasamy on the Occasion of his 80th Birthday):29-33.
- Alamdari S, Majles Ara MH, Jafar Tafreshi M. Synthesize and optical response of ZnO/CdWO₄: Ce nanocomposite with high sensitivity detection of ionizing radiations. *Optics & Laser Technology*. 2022;151:107990. <https://doi.org/10.1016/j.optlastec.2022.107990>
- He G, Fan H, Ma L, Wang K, Ding D, Liu C, et al. Synthesis, characterization and optical properties of nanostructured ZnWO₄. *Materials Science in Semiconductor Processing*. 2016;41:404-10. <https://doi.org/10.1016/j.mssp.2015.09.025>
- Singh NP, Devi YR, Singh NR, Singh NM. Synthesis of Tb³⁺ ion doped ZnWO₄ phosphors and investigation of their photoluminescence properties: concentration effect. *Bulletin of Materials Science*. 2019;42(3):96. <https://doi.org/10.1007/s12034-019-1794-4>
- Zhang J, Zhao T, Wang B, Li L, Zou L, Gan S. PEG-assisted hydrothermal synthesis and photoluminescence of CdMoO₄:Tb³⁺ green phosphor. *Journal of Physics and Chemistry of Solids*. 2015;79:14-22. <https://doi.org/10.1016/j.jpcs.2014.11.003>
- Ran W, Wang Q, Zhou Y, Ding S, Shi J, Jeong JH. Fabrication of ZnWO₄:Sm³⁺, Bi³⁺, Li⁺ with tunable white light-emitting properties for W-LEDs. *Materials Research Bulletin*. 2015;64:146-50. <https://doi.org/10.1016/j.materresbull.2014.12.050>
- Wang X, Fan Z, Yu H, Zhang H, Wang J. Characterization of ZnWO₄ Raman crystal. *Opt Mater Express*. 2017;7(6):1732-44. <https://doi.org/10.1364/OME.7.001732>
- Mazzaro R, Vomiero A. The renaissance of luminescent solar concentrators: The role of inorganic nanomaterials. *Advanced Energy Materials*. 2018;8(33):1801903. <https://doi.org/10.1002/aenm.201801903>
- Tian Y-F, Yu P, Xiao D-Q, Liu X, Xie R-S, Liu Y, et al. Photoluminescence Properties of Zinc Tungstate Films Prepared by Sol-Gel Method. *Ferroelectrics*. 2010;402(1):89-95. <https://doi.org/10.1080/00150191003708752>
- Azadmehr S, Jafar Tafreshi M, Alamdari S. Synthesis, Characterization and Scintillation Response of ZnWO₄-GO Nanocomposite. *Journal of Composites and Compounds*. 2022;4(12):158-62. <https://doi.org/10.52547/jcc.4.3.5>
- Vinayaraj S, Brijesh K, Dhanush PC, Nagaraja HS. ZnWO₄/SnO₂ composite for supercapacitor applications. *Physica B: Condensed Matter*. 2020;596:412369. <https://doi.org/10.1016/j.physb.2020.412369>
- Lou Z, Hao J, Cocivera M. Luminescence of ZnWO₄ and CdWO₄ thin films prepared by spray pyrolysis. *Journal of Luminescence*. 2002;99(4):349-54. [https://doi.org/10.1016/S0022-2313\(02\)00372-1](https://doi.org/10.1016/S0022-2313(02)00372-1)
- Li L, Yang X, Li J, Wu H, Zheng Y, Dong L. Two single-phase ZnWO₄: RE³⁺, Li⁺ (RE = Sm, Eu) white phosphors with high luminous intensity synthesized by solid-state reaction. *Journal of Luminescence*. 2020;226:117377. <https://doi.org/10.1016/j.jlumin.2020.117377>
- Li M, Takei T, Zhu Q, Kim B-N, Li J-G. Morphology Tailoring of ZnWO₄ Crystallites/Architectures and

- Photoluminescence of the Doped RE³⁺ Ions (RE = Sm, Eu, Tb, and Dy). *Inorganic Chemistry*. 2019;58(14):9432-42. <https://doi.org/10.1021/acs.inorgchem.9b01271>
20. Wu Y, Zhou S, He T, Jin X, Lun L. Photocatalytic activities of ZnWO₄ and Bi@ZnWO₄ nanorods. *Applied Surface Science*. 2019;484:409-13. <https://doi.org/10.1016/j.apsusc.2019.04.116>
 21. Mahani NM. First-principles calculations on photocatalytic activity of ZnWO₄ doped with Lithium. *Medbiotech Journal*. 2021;5:37-40.
 22. Brik MG, Nagirnyi V, Kirm M. Ab-initio studies of the electronic and optical properties of ZnWO₄ and CdWO₄ single crystals. *Materials Chemistry and Physics*. 2012;134(2):1113-20. <https://doi.org/10.1016/j.matchemphys.2012.04.003>
 23. Volokitina A, David SP, Loiko P, Subbotin K, Titov A, Lis D, et al. Monoclinic zinc monotungstate Yb³⁺, Li⁺:ZnWO₄: Part II. Polarized spectroscopy and laser operation. *Journal of Luminescence*. 2021;231:117811. <https://doi.org/10.1016/j.jlumin.2020.117811>
 24. Ding C-C, Wu S-Y, Kuang M-Q, Cheng Y-K, Zhang L-J. Theoretical studies of the local structure and spin Hamiltonian parameters for Rh²⁺:ZnWO₄. *Physica B: Condensed Matter*. 2014;451:80-3. <https://doi.org/10.1016/j.physb.2014.06.025>
 25. Wang L, Ma Y, Jiang H, Wang Q, Ren C, Kong X, et al. Luminescence properties of nano and bulk ZnWO₄ and their charge transfer transitions. *Journal of Materials Chemistry C*. 2014;2(23):4651-8. <https://doi.org/10.1039/c4tc00245h>
 26. Liao J, Zhou D, Qiu X, Liu S, Wen H-R. Charge compensation on the luminescence properties of ZnWO₄:Tb³⁺ phosphors via hydrothermal synthesis. *Optik*. 2013;124(21):5057-60. <https://doi.org/10.1016/j.jjleo.2013.03.067>
 27. Halmurat D, Yusufu T, Wang Q-I, He J, Sidike A. Rare earth ion Tb³⁺ doped natural sodium feldspar (NaAlSi₃O₈) Luminescent properties and energy transfer. *Scientific Reports*. 2019;9(1):14637. <https://doi.org/10.1038/s41598-019-51171-3>
 28. Es-soufi H, Sayyed MI, Almuqrin AH, Rajesh R, Lima AR, Bih H, et al. Crystallographic, Structural, and Electrical Properties of W⁶⁺ Substituted with Mo⁶⁺ in Crystalline Phases such as TTB Structure. *Crystals* [Internet]. 2023;13(3). <https://doi.org/10.3390/cryst13030483>
 29. Huang G, Shi R, Zhu Y. Photocatalytic activity and photoelectric performance enhancement for ZnWO₄ by fluorine substitution. *Journal of Molecular Catalysis A: Chemical*. 2011;348(1):100-5. <https://doi.org/10.1016/j.molcata.2011.08.013>
 30. Siritwong P, Thongtem T, Phuruangrat A, Thongtem S. Hydrothermal synthesis, characterization, and optical properties of wolframite ZnWO₄ nanorods. *CrystEngComm*. 2011;13(5):1564-9. <https://doi.org/10.1039/C0CE00402B>
 31. Pavithra NS, Nagaraju G, Patil SB. Ionic liquid-assisted hydrothermal synthesis of ZnWO₄ nanoparticles used for photocatalytic applications. *Ionics*. 2021;27(8):3533-41. <https://doi.org/10.1007/s11581-021-04123-9>
 32. Alharthi FA, Al-Nafaei WS, Alshayiqi AA, Alanazi HS, Hasan I. Hydrothermal Synthesis of Bimetallic (Zn, Co) Co-Doped Tungstate Nanocomposite with Direct Z-Scheme for Enhanced Photodegradation of Xylenol Orange. *Catalysts* [Internet]. 2023; 13(2). <https://doi.org/10.3390/catal13020404>
 33. Zou HY, Wang XG. Preparation and luminescence properties of ZnWO₄: Eu³⁺, Tb³⁺ phosphors. *Luminescence*. 2021;36(6):1452-8. <https://doi.org/10.1002/bio.4086>
 34. Hemmati M, Tafreshi MJ, Ehsani MH, Alamdari S. Highly sensitive and wide-range flexible sensor based on hybrid BaWO₄@CS nanocomposite. *Ceramics International*. 2022;48(18):26508-18. <https://doi.org/10.1016/j.ceramint.2022.05.347>
 35. Dehkordi NH, Alamdari S, Raeisi M. The blue-green emission color of Ag⁺, Gd³⁺ co-activated CdWO₄ phosphor via energy transfer for luminescence applications. *Physica B: Condensed Matter*. 2022;639:413969. <https://doi.org/10.1016/j.physb.2022.413969>
 36. Hosseinpour M, Abdoos H, Mirzaee O, Alamdari S. Fabrication and characterization of a new flexible ionizing ray sensor based on lead tungstate (PbWO₄). *Ceramics International*. 2023;49(3):4722-32. <https://doi.org/10.1016/j.ceramint.2022.09.362>
 37. Aliannezhadi M, Abbaspoor M, Shariatmadar Tehrani F, Jamali M. High photocatalytic WO₃ nanoparticles synthesized using Sol-gel method at different stirring times. *Optical and Quantum Electronics*. 2023;55(3):250. <https://doi.org/10.1007/s11082-022-04540-8>